J. Hydrol. Hydromech., 74, 2026, 1, 1–10
https://doi.org/10.2478/johh-2026-0001

Journal of Hydrology and Hydromechanics

Role of critical parameters on the rheology and pipeline transportation of concentrated non-Newtonian iron ore slurry

Vighnesh Prasad[1,2,*], Anil Dubey[1]

[1] Department of Pipeline Transport Systems & Societal Technologies, CSIR – Institute of Minerals & Materials Technology, Bhubaneswar, Odisha - 751013, India.
[2] Faculty of Engineering Sciences, Academy of Scientific and Innovative Research (AcSIR), CSIR - HRDG, Ghaziabad, Uttar Pradesh - 201002, India.
[*] Corresponding author. E-mail: vprasad@immt.res.in

Abstract: Achieving optimal flow characteristics while handling a complex slurry system in the pipeline needs greater attention. This study aims to demonstrate the role of iron ore concentration and size distribution on slurry rheology and their subsequent effect on slurry pipeline transportation. The concentrated iron ore slurries are sheared in the shear rate range between 0.1 – 500 s^{-1}, where the experimental data is well-represented by the Bingham-plastic model. The model parameters are employed to calculate pressure drop and energy consumption. A thorough investigation through rheo-microscopy analysis reinforces the validity of the rheological hypothesis. The rheological analysis reveals the yield-pseudoplastic flow behaviour of iron ore slurries irrespective of particle concentrations and coarse particle addition. The slurry containing iron ore fines contributes to an increase in viscosity, mitigated by introducing coarse particles. Rheo-microscopy suggests that the viscosity reduction is attributed to the obstruction of floc formation and disintegration of the slurry structure. The pressure drop and energy consumption escalate with increasing slurry velocity regardless of pipe diameters. However, these entities decrease by including coarse iron ore particles in slurries. This work advocates optimizing rheology to reduce pipeline transportation costs while handling bulk iron ore with minimum environmental repercussions.

Keywords: Iron ore; Rheology; Rheo-microscopy; Slurry pipeline transportation; Pressure drop; Specific energy consumption.

1 INTRODUCTION

The logistics of transporting large volumes of particulate solids, especially mineral ores, from extraction sites to processing plants, necessitates significant attention. Various alternative transportation methods, including trucks, trains, barges, and conveyor systems, are constrained by limitations related to the quantity of solids and the distances involved. Conversely, slurry pipelines offer several advantages, such as minimal environmental disturbance, low levels of air and noise pollution, no disruption to wildlife habitats, reduced losses during transport, easier construction and maintenance, lower operational costs, adaptability to rugged terrains, reduced carbon emissions, and insensitivity to surface conditions (Aude et al., 1974; Bose and Raju, 2001; Farris and Shrock, 1978; Kania, 1984).

Precious freshwater is used as a carrier media in slurry pipeline transportation; therefore, effort should be made to convey mineral slurries with the highest possible concentration by weight. A complex interplay of many physicochemical parameters like chemical composition, particle density, particle size distribution, pH, etc., influences the operational parameters during pipeline transportation (Larsson et al., 2012; Leong, 2021). It is well established that increasing the concentration of solids increases the viscosity (η) and yield stress (τ_y) of a mineral slurry (Mangesana et al., 2008; Singh et al., 2016; Sofrá and Boger, 2002). It increases the frictional pressure drop per km, which demands higher pump rating, pipe thickness, and specific energy consumption (SEC). All of these lead to increased capital and operational expenditure. The finer the particles and narrow the size distribution, the higher the flow resistance or η for a given particulate slurry (Chhabra and Richardson, 2011; Kaushal et al., 2005). Besides, handling highly viscous slurry due to the fineness of solids is expensive. The preparation of narrow particle size distribution from large ore lumps incurs additional costs associated with the high energy consumption during the comminution process (Mwale et al., 2005). Conversely, it is difficult to transport a slurry with coarse particles as it promotes sedimentation and degrades slurry stability. Consequently, it may lead to pipeline blockage due to the gradual deposition of coarse particles. Therefore, pipeline transportation of slurry containing only fines or coarse particles is not preferable and advisable. Another challenge in implementing pipeline transportation in industrial applications is achieving favourable flow behaviour. Therefore, conducting a thorough rheological study is crucial for characterizing the slurry before its pipeline transportation.

Researchers studied the effect of particle size distribution in a particulate slurry. Goto and Kuno (1982) reported the effect of mixing coarse and fine polystyrene particles on relative apparent viscosity in a neutrally buoyant environment. The study was conducted with 20% v/v suspension using a capillary viscometer under low and high shear rates. They found an increase in suspension viscosity when a small amount of fine particles is mixed with coarse particles. They also observed shear-thickening flow behaviour at specific fractions of coarse-fine ratios. Their work highlighted the different rheological behaviour in rotational and capillary viscometers. The same

authors also conducted studies on the effect of particle size ratios as an extension of their former study reported above (Goto and Kuno, 1984). Dabak and Yucel (1986) tried to express the interdependence of rheological parameters, namely, yield stress, flow resistance parameter, and viscosities at low and high shear rates in the form of several non-dimensional parameters dependent on the physical properties of the slurry. The properties considered were particle size distribution, slurry concentration, particle density, and particle shape factor.

Assefa and Kaushal (2017) also developed an empirical model to compute the viscosity of particulate Bingham slurries based on the physical properties of the slurry, including solid volume fraction, maximum solid volume fraction, median particle diameter, and coefficient of uniformity. Ohki et al. (1996) studied the effect of particle size distribution and additives in forming coal-water slurries. They stated that the water content adsorbed by the coal sample entraps within the voids of the coal particles and, hence, does not contribute to the flow. The particle size distribution, which retains more immobilized liquid, forms a more viscous slurry. Senapati and Mishra (2012) showed how blending coarse bottom ash with fine fly ash slurry reduces the shear stress at a given shear rate for all solid concentrations. In another study, Senapati et al. (2013) carried out pipe loop studies in 50 mm NB pipelines and demonstrated the reduction in head loss by blending a small percentage of coarse bottom ash particles in the fly ash slurry. Rawat et al. (2019) thoroughly studied the rheological behaviour of different fly ash samples generated from various coal-based thermal power plant ESP fields. Usually, the fly ash generated and collected from the 1st ESP has the largest mean particle size, which decreases with downstream ESPs. They showed that mixing various fly ash samples enables them to increase the solid loading in the slurry systems, which can be conveyed with a marginal increase in the head loss. Researchers (Liu et al., 2021; Zhao et al., 2024; Senapati et al., 2019; Singh et al., 2021) also reported that the limestone, coal and silica slurries show different rheological behaviour with monomodal, bimodal, and multimodal particle size distributions. The authors demonstrated that bimodal and multimodal size distributions exhibit lower yield stress and viscosity than monomodal distributions. Prasad et al., (2019) thoroughly investigated the effects of blending coarse coal ash particles in fine coal ash slurry samples in various fractions. They explained that the coarse coal ash hinders the formation of flocs by fine coal ash particles, causing a reduction in the slurry viscosity.

The author also witnessed varying rheological behaviour for the same size distribution and particle concentration collected from different sources (Au and Leong, 2016; Ndlovu et al., 2011). They further indicated that the mineralogical discrepancy in the sample also influences the slurry rheology. Furthermore, the particle surface charge also plays a vital role in changing the rheological properties (Au and Leong, 2016; Larsson et al., 2012), mainly depending on the slurry pH. Hence, a wide range of options is available to tune the rheology of a given slurry system to achieve a high-concentration slurry with minimum possible viscosity, yield stress, and favorable flow behavior while conveying through the slurry pipeline.

It is worth noting that the rheological signatures drastically vary when solid loading in a continuous medium exceeds 60 wt.%. The rheological investigation of such highly concentrated and complex slurry systems is still inadequate in the reports. Besides, microscopy justification of the experimental data is one area that supports, validates, and explains the rheological phenomena in the slurry systems, which is missing in the published literature. Many researchers have reported the role of blending coarse and fine particles in the rheology of a slurry/suspension. However, determining critical coarse concentration above which the flow behaviour doesn't improve appreciably has not been discussed sufficiently in the previous works. Most of the investigators have focused on the influencing parameters of slurry rheology; however, the rheological role in quantifying the pipe flow of a non-Newtonian slurry system has rarely been attempted in the past.

In the present investigation, iron ore is taken as a test sample. India is on an ambitious path to achieve 300 MT of steel production capacity by 2030-31 as per the New Steel Policy 2017 (Irfan et al., 2023). Approximately 1.65 tons of iron ore is required to produce 1 tonne of steel (Holmes et al., 2022). This ratio may vary depending on the grade of iron ore and the production process employed. The present work demonstrates the rheological behaviour of a concentrated iron ore slurry with increasing solid concentration and a fraction of coarse particles. A detailed rheo-microscopy analysis further endorses the rheological hypothesis. The pressure drop and energy consumption have been estimated using Bingham model correlations. Results advocate that the high-concentration fine particle slurry can act as a carrier media for coarse particles due to its increased viscosity. This work addresses the rheological and pipe flow challenges of iron ore slurries by adopting a bi-modal particle size distribution. An optimum concentration of coarse particles in the fine slurry has been estimated, which supports minimum viscosity, yield stress, start-up pressure, pressure drop, and specific energy consumption.

2 MATERIAL AND METHODS

2.1 Sample collection and slurry preparation

he iron ore samples were from National Mineral Development Corporation Ltd., Chhattisgarh, India. These samples were milled in a planetary ball mill (BM1200, Micromatic Technologies) to obtain two different particle size distributions: fine and coarse.

The samples were dried in a laboratory oven (TI-128 B, TEMPO) at 105°C for 60 minutes to eliminate moisture. DI water was used as a continuous phase to prepare the 60 – 75 wt.% iron ore slurries. The slurry density, ρ_m (kg/m^3), was estimated using Equation (1) (Prasad, 2024), and tabulated in Table 1.

$$\rho_m = \frac{100}{\left(\frac{C_W}{\rho_S} + \frac{100 - C_W}{\rho_l}\right)} \quad (1)$$

Here, ρ_s and ρ_l are the density of iron ore (4574 kg/m^3) and water (1000 kg/m^3), respectively. C_w is the concentration of iron ore by wt.%.

Table 1. Slurry densities at varying iron ore concentrations.

Iron ore concentration by weight, Cw (wt.%)	60	65	70	75
Slurry density, ρ_m (kg/m^3)	1882.6	2032.1	2207.3	2415.6

2.2 Shear rheology experiments

The rheological experiments were performed using a Rotational Rheometer (MCR 302e, Anton Paar Ltd.). The slurries were sheared in the shear rate ($\dot{\gamma}$) range between 0.1 – 500 s^{-1}. Conducting rheological tests of settling slurries in the low shear rate regime is challenging, especially when the slurries containing coarse and heavy particles. Therefore, precautions

were taken in this study to prevent particle settling. The iron ore concentration was maintained above 60 wt.%, which is considered a high-concentration slurry system where particles do not settle quickly due to the hindered settling effect (Baas et al. 2022; Li and Zyl 2022; Zhu et al. 2018) Additionally, the fine iron ore slurry (d_{50} = 12.3 µm) exhibits high viscosity (Figure 3), creating a high-viscosity carrier medium that supports the weight of the coarse particles (d_{50} = 173.9 µm). A vane shear tool (ST22-4V40) with a pre-shear rate of 50 s^{-1} for 60 seconds was also applied during the rheological measurements to further prevent particle settling.

All experiments were conducted at a temperature of 25°C, as it serves as a practical and scientifically neutral reference condition, universally accepted as the standard laboratory ambient temperature for rheological measurements. By conducting tests at 25°C, we can minimize uncontrolled thermal effects and isolate true compositional or shear-dependent behaviour.

2.2 Shear rheology experiments

The rheo-microscope studies were carried out with the rheometer using a profiled parallel plate geometry (PP25/P2). The slurry was placed between the rough plate and a fixed glass plate with a diameter of 50 mm by maintaining a gap of 1 mm. A light source and a lens of 10x magnification were installed just below the fixed glass plate. A CCD camera captured the deformation of slurry under shear. A passive hood was used to avoid sample evaporation during experiments. The microscopy experiments were performed at 10 wt.% iron ore concentration and at $\dot{\gamma}$ = 10 s^{-1}, as slurry microstructures were not traceable and captured above these conditions.

2.2 Shear rheology experiments

The Image J software was used to quantify the total area occupied by the iron ore aggregates in a 2D image. The procedure includes a) Converting the raw image to an 8-bit image, b) setting the measurement scale, c) threshold adjustment of the image, and d) analyzing the aggregates in the occupied area. The total area (%), A_T is estimated using Equation (2) (Kulkarni et al., 2017)

$$A_T = \left(\frac{\text{Total area occupied by iron ore aggregates in a 2D image}}{\text{Total area of the 2D image}}\right) \times 100 \qquad (2)$$

3 RESULTS AND DISCUSSION

3.1 Characterization of iron ore

The particle size distribution (PSD) of two sets of iron ore samples, analyzed through a particle size analyzer (LA-960, HORIBA), are shown in Figure 1a. Both possess broad particle size distribution, with median particle size, d_{50} = 12.3 µm and d_{50} = 173.9 µm, designated as fine and coarse iron ore, respectively. A Field Emission Scanning Electron Microscopy, FE-SEM (SUPRA 55, Carl Zeiss) was used to evaluate the morphology and shape of the collected iron ore sample (Figure 1b). As observed, it consists of irregularly and aggregated shaped solid particles. The X-ray Fluorescence Spectrometer, XRF (ZETIUM 4.0, Malvern Panalytical) confirms that Fe_2O_3, Al_2O_3 and SiO_2 are in abundance with small fractions of the oxides of Mn, Ti, Ca, K, S, P, Mg, and Cr in iron ore sample (Figure 1c). The specific gravity (Ss) of the iron ore sample was estimated as per IS: 2386, Part-3 (Standard, 1963) using a pycnometer (Borosil Ltd.) and found to be 4.574.

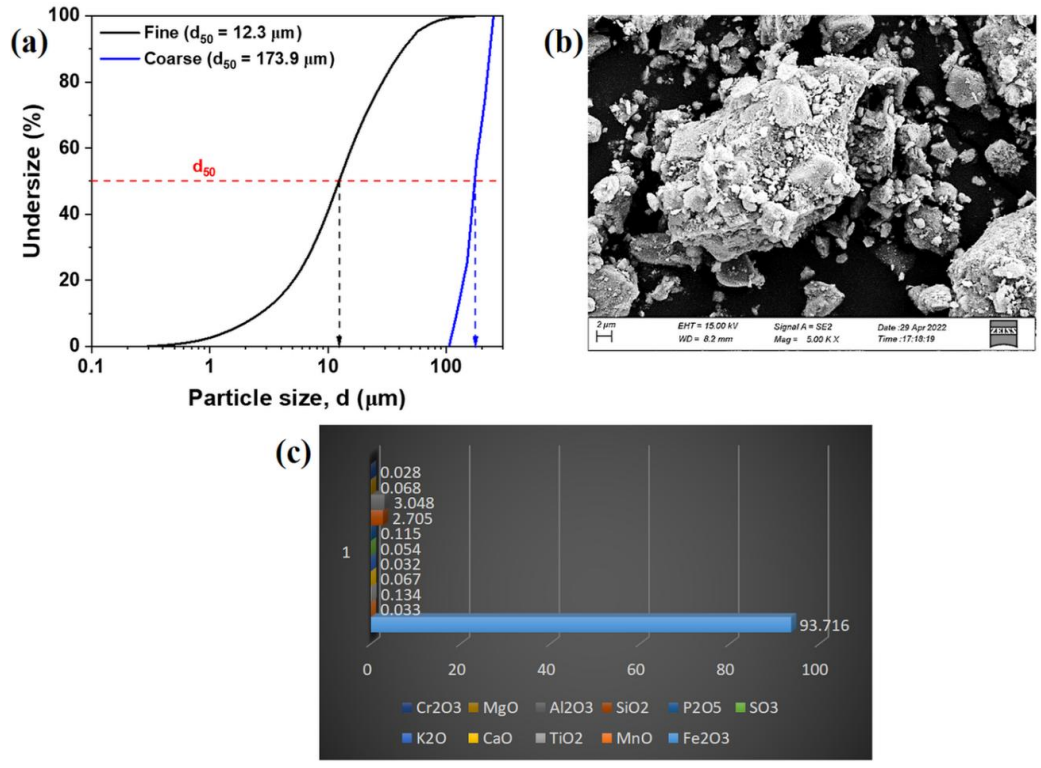

Fig. 1. (a) Particle size distribution; (b) SEM image at 5000x; (c) Chemical composition.

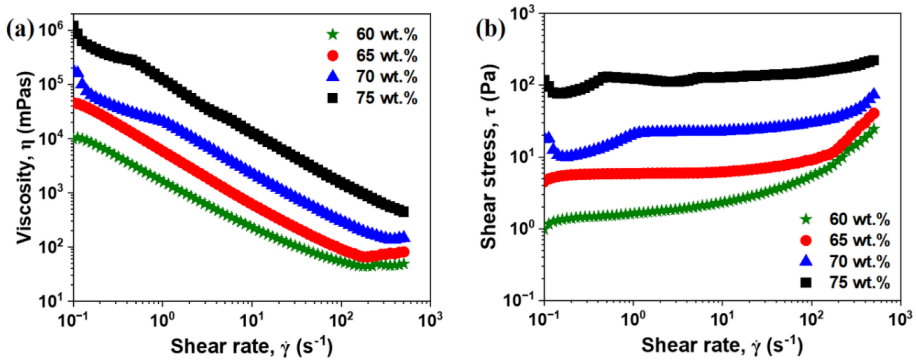

Fig. 2. Flow curves of 60 – 75 wt.% iron ore (d_{50} = 12.3 µm) slurries (a) Viscosity versus shear rate curves (b) Shear stress versus shear rate curves.

3.2 Rheological studies

3.2.1 Effect of iron ore concentration

The flow curves of 60–75 wt.% iron ore (d_{50} = 12.3 µm) slurries are presented in Figure 2. As evident, the apparent slurry viscosity (η) and shear stress (τ) increase with increase in iron ore concentrations (C_w). The increase in η is in the order of ~ 10^2 with +15% addition of iron ore in the 60 wt.% slurry. The increase in η is attributed to the increase in inter-particle interactions with an increase in iron ore loading. The shear thinning flow behaviour prevails regardless of iron ore concentration in the carrier water, which is explained by the decrease in η with applied $\dot{\gamma}$. Researchers have proposed that solid particles within a suspension can hold certain amounts of immobilized liquid at low $\dot{\gamma}$ (He et al., 2006). As $\dot{\gamma}$ rises, this liquid is progressively released, promoting the movement of the particles along the flow direction and contributing to a decrease in η. Previous work also reports that the increase in $\dot{\gamma}$ leads to the breakdown of floc structures into an array of particles that align with the flow direction with applied $\dot{\gamma}$ (Prasad et al., 2019). The findings imply that transporting a slurry containing 75 wt.% iron ore fines may lead to substantial pumping expenses owing to its highly viscous characteristics.

3.2.2 Effect of incorporating coarse particles in fine iron ore slurries

In this set of experiments, 0-50 wt.% coarse iron ore (d_{50} = 173.9 µm) particles were added in fine iron ore (d_{50} = 12.3 µm) slurries such that the total iron ore content in the slurries remained 75 wt.% (Figure 3). The data presented in Figure 3 indicates that the 75 wt.% iron ore slurries display shear thinning flow behavior, irrespective of incorporating coarser particles into the fine iron ore slurry. In addition, η of the slurry is reduced upon the addition of coarse iron ore particles, as illustrated in Figure 3a.

The non-monotonic flow behaviour in Figures 2b and 3b is the result of microstructural transitions and particle migration within the concentrated iron ore slurries. These rheological signatures are common in yield stress fluids where local maxima and minima appear when the internal network structure is partially built and collapses with increasing shear rate (Coussot 2014). Similarly, Luo and Ingrid (2018) suggested that particles temporarily form hydroclusters within slurry systems, increasing local stress (local maximum), followed by breakup of clusters at higher shear (local minimum). Phillips et al. (1992) noted that increasing shear causes particle migration in slurry/suspension, resulting in a local concentration gradient that can be identified as local minima and maxima in flow curves.

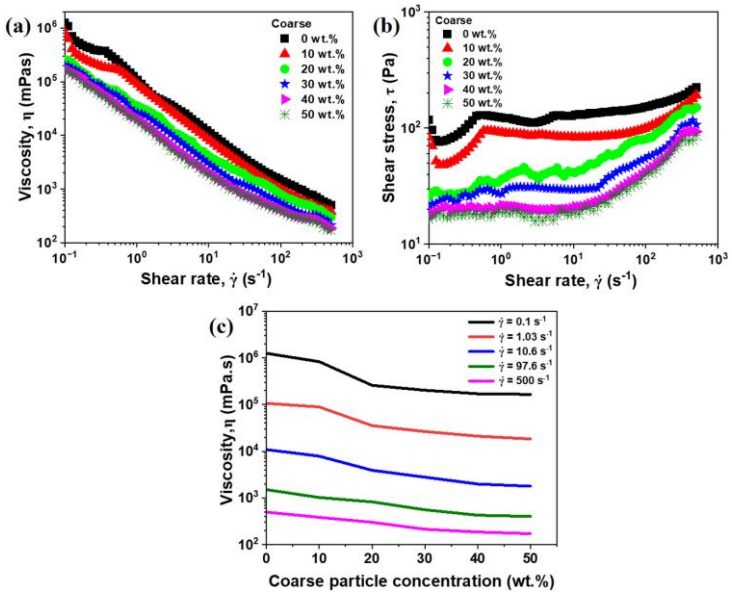

Fig. 3. Flow curves of 75 wt.% iron ore (d_{50} = 12.3 µm) slurries with varying coarse iron ore (d_{50} = 173.9 µm) particles from 0 – 50 wt.% (a) Viscosity versus shear rate curves (b) Shear stress versus shear rate curves; (c) Effect of coarse iron ore (d_{50} = 173.9 µm) particles on viscosity of 75 wt.% fine iron ore (d_{50} = 12.3 µm) slurries.

Notably, beyond the inclusion of 30 wt.% coarse particles, no considerable decrease in η is observed (Figure 3c). Comparable qualitative findings have been documented in a research concerning South Australian coal slurries (Logos and Nguyen, 1996), where the authors determined that the addition of a critical concentration of coarse particles to fine slurry does not lead to any significant alteration in η, attributed to the complete breakdown of the dense slurry structure. These findings explain that η of highly concentrated iron ore slurry can be diminished by blending an optimal fraction of coarse iron ore particles.

Furthermore, the rheological interpretations are supported by the results obtained from the rheo-microscope, where 0-50 wt.% coarse iron ore (d_{50} = 173.9 µm) particles are incorporated in 10 wt.% fine iron ore (d_{50} = 12.3 µm) slurry, ensuring that the total solid content (fine and coarse) remains at 10 wt.%. For instance, Figure 4d illustrates that the 10 wt.% iron ore slurry comprises 30% coarse and 70% fine particles within the overall iron ore concentration.

In the absence of $\dot{\gamma}$, the 10 wt.% iron ore slurry containing particles of d_{50} = 12.3 µm develops a tightly packed floc structure (Figure 4a). This structure progressively transforms into more loosely arranged formations with increased void spaces with increasing fraction of coarser iron ore (d_{50} = 173.9 µm) particles, as shown in Figures 4b–f. Consequently, this leads to a reduction in the viscosity of the slurry. Interestingly, the microstructure does not alter above the addition of 30 wt.% coarse iron ore particles, indicating that viscosity does not experience a significant reduction (Figure 4d–f).

Moreover, the procedure for determining the total area occupied by iron ore aggregates (A_T) is specified in section 2.4. Figures 5a–f show that A_T declines from 99.9% to 72.9% with computing 0-50 wt.% coarse iron ore particles to the fine slurries. This phenomenon implies that the coarse iron ore particles disrupt the dense floc structure, creating larger voids, which is reflected in the lower A_T value. After surpassing 30 wt.% of coarse iron ore addition, the variation in A_T is marginal.

A comparable observation is noted when the same slurries are subjected to $\dot{\gamma}$ = 10 s^{-1} (Figure 6a–f). In this scenario, the breakdown of dense flocs is influenced by both the shear force and the presence of larger particles, resulting in a markedly greater deformation of the slurries (Figure 6a–f) in contrast to the condition without shear (Figure 4a–f).

The critical concentration for coarse particles has been identified as 30 wt.%, even when subjected to $\dot{\gamma}$ = 10 s^{-1}. Beyond this concentration, the microstructure of the slurry appears qualitatively consistent despite the further addition of coarse particles (Figure 6d–f). This observation indicates that viscosity decreases gradually until the 30 wt.% threshold is reached, after which changes in viscosity are minimal, as also demonstrated in the rheological curve (Figure 3c). Besides, the lower magnitudes of A_T (72.6 – 42.8 %) after applying a $\dot{\gamma}$ of 10 s^{-1} on 10 wt.% iron ore slurries suggest a more pronounced disintegration of the slurry structure, as illustrated in Figure 7.

3.2.3 Model fitting on the rheological data

The well-known Bingham plastic model (Equation 3) (Chhabra and Richardson, 2011) best fits the experimental data, as shown in Figure 8. The parameters derived from this fitting process, namely the shear yield stress (τ_y) and Bingham viscosity (η_B), are presented in Table 2.

$$\tau = \begin{cases} \tau_y + \eta_B.\dot{\gamma} & \text{for} \quad \tau \geq \tau_y \\ \dot{\gamma} = 0 & \text{for} \quad \tau < \tau_y \end{cases} \tag{3}$$

Table 2. Rheological parameters while fitting of Bingham plastic model.

Coarse (wt.%)	τ_y (Pa)	η_B (Pa.s)	R^2	RMSE (Pa)
0	131.55	0.28	0.99	1.85
10	78.90	0.24	0.99	1.08
20	52.14	0.22	0.94	5.60
30	32.19	0.19	0.96	3.12
40	22.23	0.18	0.96	3.69
50	20.98	0.15	0.95	4.23

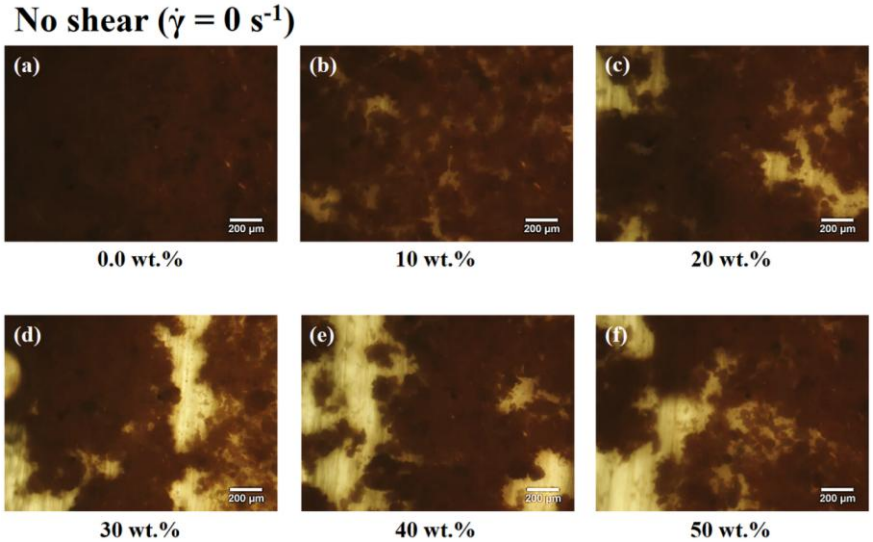

Fig. 4. Rheo-microscopy images of 10 wt.% iron ore (d_{50} = 12.3 µm) slurry with varying coarse iron ore (d_{50} = 173.9 µm) particles from 0–50 wt.% at $\dot{\gamma}$ = 0 s^{-1}.

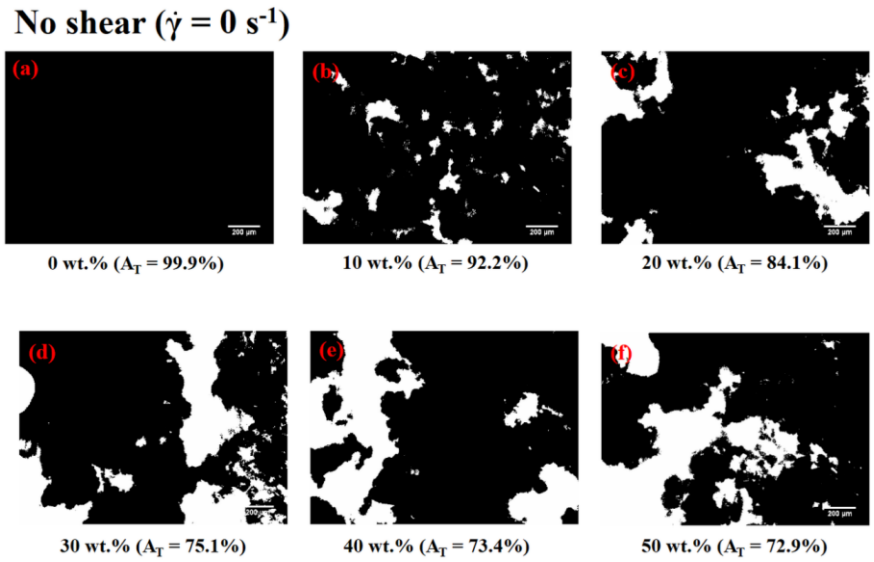

Fig. 5. Estimation of total area occupied by the particle aggregates (A_T) using Image J in 10 wt.% iron ore (d_{50} = 12.3 μm) slurry with varying coarse iron ore (d_{50} = 173.9 μm) particles from 0-50 wt.% at $\dot{\gamma}$ = 0 s^{-1}.

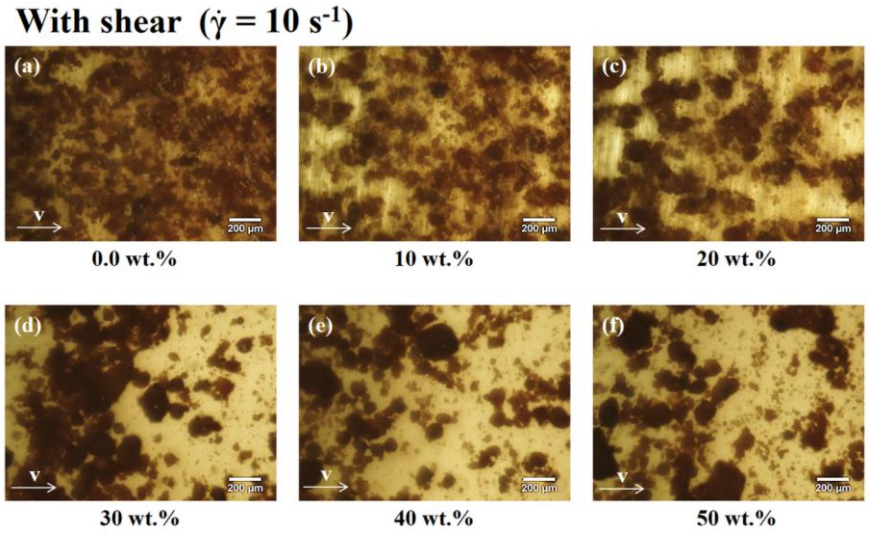

Fig. 6. Rheo-microscopy images of 10 wt.% iron ore (d_{50} = 12.3 μm) slurry with varying coarse iron ore (d_{50} = 173.9 μm) particles from 0–50 wt.% at $\dot{\gamma}$ = 10 s^{-1}.

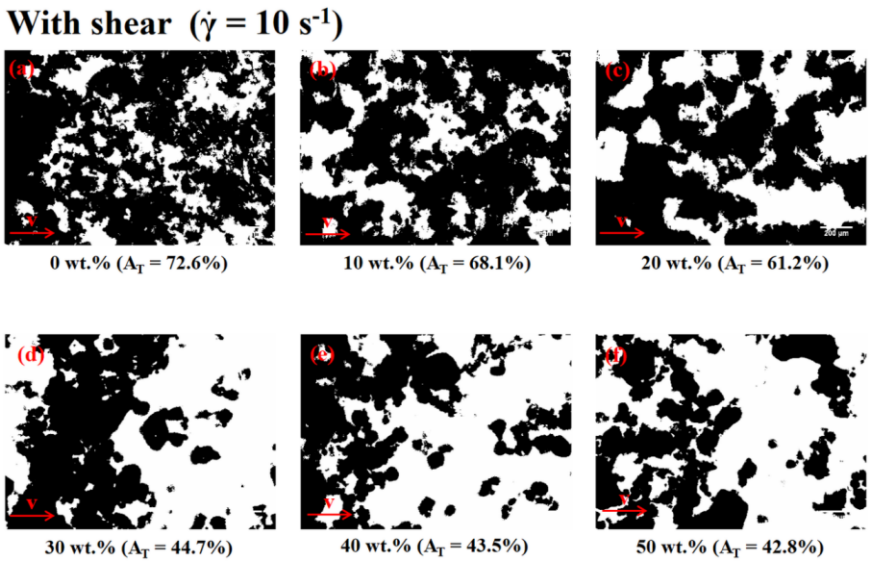

Fig. 7. Estimation of total area occupied by the particle aggregates (A_T) using Image J in 10 wt.% iron ore (d_{50} = 12.3 μm) slurry with varying coarse iron ore (d_{50} = 173.9 μm) particles from 0–50 wt.% at $\dot{\gamma}$ = 10 s^{-1}.

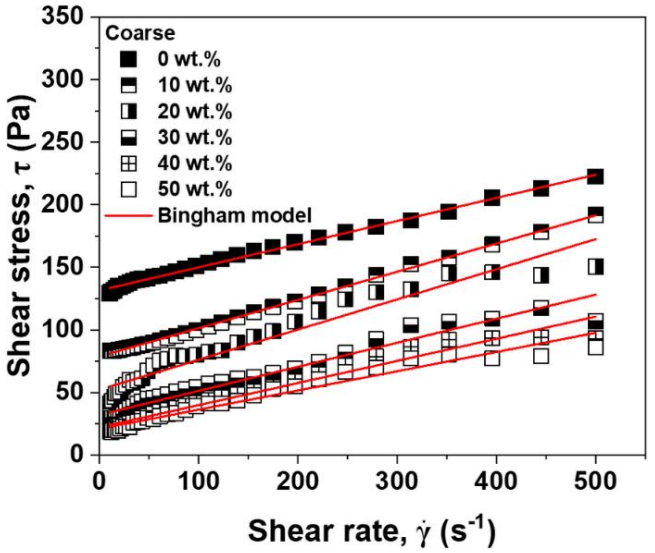

Fig. 8. Bingham plastic model fitting on the rheological data of 75 wt.% iron ore (d_{50} = 12.3 µm) slurries with varying coarse iron ore (d_{50} = 173.9 µm) particles from 0–50 wt.%.

Figure 8 and Table 2 show that the higher regression coefficient indicates the best fitting of experimental data with the Bingham plastic model. The RMSE value suggests that the fitted Bingham rheological model deviates by ≤ 5.6 Pa from the measured shear stress values, where the stress values vary between ~ 17 – 222 Pa, which may be considered an acceptable fit to the model. Therefore, these iron ore slurries can be considered as Bingham plastic slurries. τ_y is the threshold stress needed to start or maintain a fluid flow. Besides, η_B is the slope of the $\dot{\gamma} - \tau$ curve, which should be low for obtaining a favourable flow in the pipeline.

As evident in Figure 9a, τ_y exponentially decreases with an increase in coarse particle concentration in 75 wt.% fine iron ore slurry. Adding coarse particles in a fine slurry is believed to weaken the inter-particle structure, which requires lesser shear force to break down the structure and initiate the flow. The low magnitude of τ_y translates to the less pumping energy needed for transporting the iron ore slurry through the pipeline. In addition, the start-up pressure (P_{st}), which is the minimum pumping pressure necessary to transition the static liquid from a state of rest to its operational velocity, is calculated using τ_y for various pipe lengths (L) and diameters (D), as articulated in Equation (4) (Michaelides et al., 2016).

$$P_{st} = \frac{4\tau_y L}{D} \tag{4}$$

The data demonstrate that P_{st} per meter length of pipe declines exponentially with rising concentrations of coarse particles, regardless of D (Figure 9b). The slurry pipeline system often undergoes temporary shutdowns due to issues such as breakdowns of conveying mechanisms, non-operational electronic components, and scheduled maintenance activities. In this scenario, P_{st} serves as an indicator of the pumping pressure needed to restart the slurry flow after the system has been halted. The current findings suggest that notably lower pumping energy is necessary to initiate the flow of concentrated slurry in the presence of coarse particles. Furthermore, a comparatively high pumping pressure is required to convey iron ore slurry in pipes with smaller diameters.

3.3 Slurry flow calculation

The parameters outlined in Table 2 are employed to calculate the Reynolds number (Re_B), critical Reynolds number (Re_{Bc}), Hedstrom number (He), total friction factor (f), head loss (h_L), and specific energy consumption (SEC) during the transport of 75 wt.% iron ore fines mixed with coarse particles in D = 0.1 – 0.5 m at slurry velocity (v_m) = 2–5 m/s. The Reynolds number (Re_B) and Hedstrom number (He) for Bingham plastic fluids are estimated using Equations (5) and (6) (Abulnaga, 2002; Darby and Chhabra, 2016).

$$\mathrm{He} = \frac{D^2 \tau_y \rho_m}{\eta_B^2} \tag{5}$$

$$\mathrm{Re}_B = \frac{D v_m \rho_m}{\eta_B} \tag{6}$$

Hanks and Pratt (Hanks, 1967) conducted a comprehensive analysis of experimental data concerning critical Reynolds numbers (Re_{Bc}) and introduced a correlation between Re_B and He, as expressed in Equation (7).

$$\mathrm{Re}_{Bc} = \frac{\mathrm{He}}{8x_c}\left(1 - \frac{4}{3}x_c + \frac{1}{3}x_c^4\right) \tag{7}$$

Here, X_c is the ratio of the yield stress to the wall shear stress, which can be expressed in Equation (8) (Abulnaga, 2002).

$$\frac{x_c}{(1-x_c)^3} = \frac{\mathrm{He}}{16800} \tag{8}$$

When $Re_B < Re_{Bc}$, the slurry flow is considered as laminar, and the laminar friction factor (f_L) is estimated using Equation (9) (Darby and Chhabra, 2016; Swamee and Aggarwal, 2011).

$$\frac{1}{\mathrm{Re}_B} = \frac{f_L}{16} - \frac{\mathrm{He}}{6\mathrm{Re}_B^2} + \frac{\mathrm{He}^4}{3f_L^3 \mathrm{Re}_B^8} \tag{9}$$

In the case of $Re_B > Re_{Bc}$, the flow lies in a turbulent regime, and the turbulent friction factor (f_T) is determined using Equations (10) and (11) (Darby and Chhabra, 2016; Darby and Melson, 1981).

$$f_T = 10^c \mathrm{Re}_B^{-0.193} \tag{10}$$

$$c = -1.378\left\{1 + 0.146\exp\left(-2.9\times10^{-5}\mathrm{Re}_B\right)\right\} \tag{11}$$

A comprehensive equation for the explicit friction factor (f) is proposed that is applicable across all flow regimes, which is presented in Equations (12) and (13) (Assefa and Kaushal, 2014; Darbya and Melson, 1981).

$$f = (f_L^m + f_T^m)^{\frac{1}{m}} \tag{12}$$

$$m = 1.7 + \frac{40000}{\mathrm{Re}_B} \tag{13}$$

Head loss, expressed in meters of water column per meter of pipe length (h_L in mWc/m), pressure drop (Δp in bar/km), specific energy consumption (SEC in kWh/t-km) - energy needed to convey the slurry, and solid volume fraction (ϕ) are estimated using Equations (14) - (17), respectively (Brown and Heywood, 1991; Prasad, 2024).

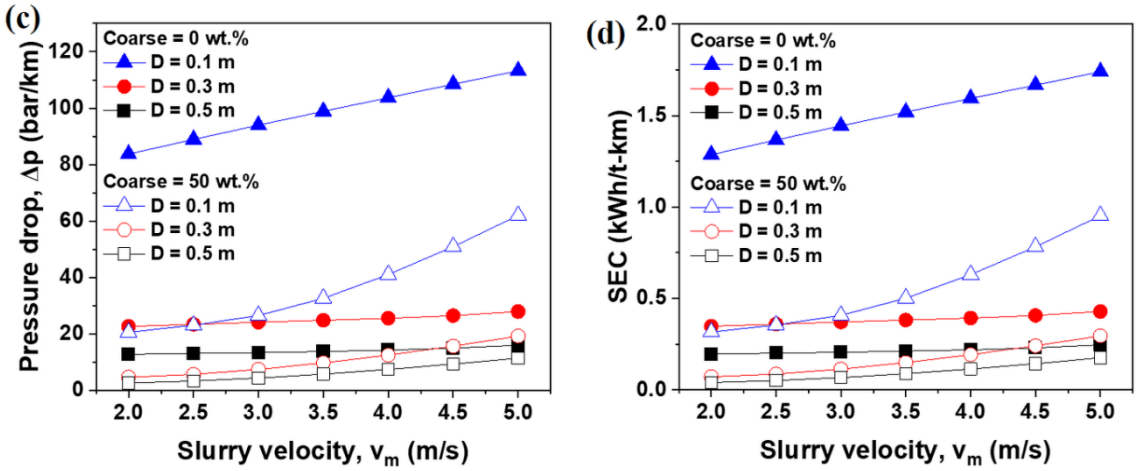

Fig. 10. variation of Δp and SEC with v_m in 75 wt.% fine iron ore slurries (a and b) At varying coarse particle concentration (0-50 wt. %); (c and d) At varying D = 0.1 – 0.5 m.

$$h_L = \frac{2.f.v^2{}_m}{gD}\left(\frac{\rho_m}{\rho_l}\right) \quad (14)$$

$$\Delta p = \rho_l.g.h_L \quad (15)$$

$$\text{SEC}\left(\frac{kWh}{t-km}\right) = \frac{2.73h_L}{\phi S_s} \quad (16)$$

$$\phi = \frac{\left(\frac{C_w}{\rho_s}\right)}{\left(\frac{C_w}{\rho_s}+\frac{100-C_w}{\rho_l}\right)} \quad (17)$$

As shown in Figures 10 (a, b), pressure drop (Δp) and SEC increase with v_m regardless of coarse particle addition and D. Pressure drop and SEC increase from 12.8 bar/km and 0.19 kWh/t-km to 16 bar/km and 0.24 kWh/t-km, respectively, when v_m is varied between 2 – 5 m/s while conveying 75 wt.% fine iron ore slurry in a pipe of D = 0.5 m (Figures 10 (a, b)). The findings suggest that maintaining a higher velocity in a slurry pipeline can lead to increased energy requirements for pumping and a greater risk of pipe erosion wear, thereby contributing to an overall rise in transportation and maintenance costs. Interestingly, Δp and SEC can be minimized up to ~ 70% by adding 30 wt.% of coarse iron ore particles to the fine slurry flowing at v_m = 2 m/s in D = 0.5 m. No significant reduction in Δp and SEC is noticed after 30 wt.% of coarse iron ore addition in the fine slurry (Figures 10 (a, b)).

Moreover, smaller pipe diameters can be chosen to reduce the capital cost associated with pipe material. However, Δp and SEC possess higher values in small pipes. Δp and SEC are noted to be 83.72 bar/km and 1.28 kWh/t-km, when 75 wt.% fine iron ore slurry is conveyed at v_m = 2 m/s in a small pipe of D = 0.1 m (Figures 10 (c, d)). Interestingly, a reduction up to ~ 75% of Δp and SEC has been observed when 50 wt.% coarse iron ore particles are added to the fine slurry for the same flow condition and pipe size.

4 CONCLUSIONS

The incorporation of 60 - 75 wt.% fine iron ore (d_{50} = 12.3 µm) in carrier water leads to a viscous slurry. The shear thinning flow behaviour is consistently maintained regardless of iron ore loading, which is considered a favourable flow behaviour in the pipeline. Interestingly, the high η associated with 75 wt.% fine iron ore slurries is significantly reduced by adding 0 - 50 wt.% coarse iron ore particles (d_{50} = 173.9 µm), preserving the shear thinning flow characteristics. The reduction of η with coarse particle addition and applied $\dot{\gamma}$ is due to the transition from a densely packed structure to a loosely arranged configuration and breakdown of dense floc structure. High R^2 and low RMSE values observed while fitting Bingham plastic model emphasizes the importance of τ_y in the iron ore slurry systems. The presence of coarse iron ore particles hinders the formation of the robust network structure of fine particle slurries, causing an exponential decrease in τ_y and P_{st}.

Results also indicate that Δp and SEC are the functions of v_m, recommending against the operation of the slurry pipeline at high v_m. Moreover, the higher magnitude of Δp and SEC during conveying of 75 wt.% fine iron ore slurry can be reduced by employing a critical concentration of coarse particles, which is determined as 30 wt.% in the present investigation. Above this critical threshold, the change in η, Δp and SEC with applied $\dot{\gamma}$ and v_m is negligible. The hydraulic conveying of the iron ore through smaller pipe diameters tends to incur higher pumping costs due to increased values of Δp and SEC; however, the integration of coarse particles can enhance the economic viability of the process, even with the same small diameter pipes. Our findings demonstrate that a favourable flow behaviour with reduced pumping and pipe material costs is feasible by adopting a bi-model size distribution in the iron ore slurry systems during pipeline transportation.

Acknowledgment: The Science and Engineering Research Board, New Delhi supports this work under project No. EEQ/2022/000101. The authors thank the Director, CSIR – IMMT Bhubaneswar, for permitting them to publish this work. The authors are also thankful to the characterization division of CSIR - IMMT Bhubaneswar for providing SEM, EDS, XRF, and XRD facilities.

REFERENCES

Abulnaga, B., 2002. Slurry systems handbook, New York: McGraw-Hill.

Assefa, K.M., Kaushal, D.R., 2017. A new model for the viscosity of highly concentrated multi-sized particulate Bingham slurries. Part. Sci. Technol. 35, 77–85. https://doi.org/10.1080/02726351.2015.1131789

Assefa, K.M., Kaushal, D.R., 2014. A comparative study of friction factor correlations for high concentrate slurry flow in

smooth pipes. J. Hydrol. Hydromechanics 63. https://doi.org/10.1515/johh-2015-0008

Au, P.I., Leong, Y.K., 2016. Surface chemistry and rheology of slurries of kaolinite and montmorillonite from different sources. KONA Powder Part. J. 2016, 17–32. https://doi.org/10.14356/kona.2016007

Aude, T.C., Thompson, T.L., Wasp, E.J., 1974. Economics of slurry pipeline system. In: Fifteenth Annual Meeting of Transportation Research Forum; Theme- Transportation in Focus. 1st ed. San Francisco, 194–202.

Baas, J.H., Baker, M.L., Buffon, P., Strachan, L.J., Bostock, H.C., Hodgson, D., Eggenhuisen, J.T., Spychala, Y.T., 2022. Blood, lead and spheres: A hindered settling equation for sedimentologists based on metadata analysis. The Depositional Record, 2, 603-615. https://doi.org/10.1002/dep2.176

Bose, A.N., Raju K.S., 2001. Slurry transportation in Indian mines, Ministry of Mines, Govt. of India: 8–17.

Brown, N., Heywood, N., 1991. Slurry Handling: Design of solid-liquid systems. Springer Science & Business Media, London.

Chhabra, R., Richardson, J., 2011. Non-Newtonian flow and applied rheology: engineering applications. Butterworth-Heinemann.

Coussot, P., 2014. Yield stress fluid flows: A review of experimental data. J. Non-Newtonian Fluid Mech. 211, 31-49. https://doi.org/10.1016/j.jnnfm.2014.05.006

Dabak, Y., Yucel, O., 1986. Shear viscosity behavior of highly concentrated suspensions at low and high shear-rates, Rheol Acta 25, 527-533.

Darby, R., Chhabra, R., 2016. Chemical engineering fluid mechanics. CRC Press.

Darbya, R., Melson, J., 1981. How to predict the friction for flow of Bingham plastics. Chem Engg. 88.

Farris, M., Shrock, D., 1978. The Economics of Coal Slurry Pipelining: Transportation and Non-Transportation Factors. Transp. J. 18, 45-57.

Goto, H., Kuno, H., 1984. Flow of Suspensions Containing Particles of Two Different Sizes through a Capillary Tube. II. Effect of the Particle Size Ratio. J. Rheol. 28, 197-205. https://doi.org/10.1122/1.549740

Goto, H., Kuno, H., 1982. Flow of Suspensions Containing Particles of Two Different Sizes through a Capillary Tube. J. Rheol. 26, 387-398. https://doi.org/10.1122/1.549682

Hanks, R.W., 1967. On the Flow of Bingham Plastic Slurries in Pipes and Between Parallel Plates. Soc. Pet. Eng. J. 7, 342-346. https://doi.org/10.2118/1682-pa

He, M., Wang, Y., Forssberg, E., 2006. Parameter studies on the rheology of limestone slurries. Int. J. Miner. Process. 78, 63–77. https://doi.org/10.1016/j.minpro.2005.07.006

Holmes, R.J., Lu, Y., Lu, L., 2022. Introduction: Overview of the global iron ore industry. Iron Ore Mineral. Process. Environ. Sustain. 1–56. https://doi.org/10.1016/B978-0-12-820226-5.00023-9

Irfan, D., Varadharajan, S., Mateen, S., Mobasshir, S.M., Kumar, A., Shukla, B.K., 2023. Study of Growth of Steel, Steel Infrastructure and Steel Industries in India, in: AIP Conference Proceedings. https://doi.org/10.1063/5.0163369

Kania, J.J., 1984. Economics of coal transport by slurry pipeline versus unit train. A case study. Energy Econ. 6, 131–138. https://doi.org/10.1016/0140-9883(84)90028-8

Kaushal, D.R., Sato, K., Toyota, T., Funatsu, K., Tomita, Y., 2005. Effect of particle size distribution on pressure drop and concentration profile in pipeline flow of highly concentrated slurry. Int. J. Multiph. Flow 31, 809–823. https://doi.org/10.1016/j.ijmultiphaseflow.2005.03.003

Kulkarni, S., Verma, A., Mishra, N.S., Thareja, P., 2017. Partitioning and self assembly of silica and hematite particles at grain boundaries of hexagonal liquid crystals: Implications on rheology. J. Rheol. 61, 311-25. https://doi.org/10.1122/1.4975333

Larsson, M., Hill, A., Duffy, J., 2012. Suspension stability: Why particle size, zeta potential and rheology are important Product Technical Specialists Rheometry Products Malvern Instruments Limited. Annu. Trans. Nord. Rheol. Soc. 20, 6-12.

Leong, Y.K., 2021. Controlling the rheology of iron ore slurries and tailings with surface chemistry for enhanced beneficiation performance and output, reduced pumping cost and safer tailings storage in dam. Miner. Eng. 166, 106874. https://doi.org/10.1016/j.mineng.2021.106874

Li, Y., Zyl, D., 2022. Hindered settling of flocculated multi-sized particle suspension, part I: Segregation mechanism of non-flocculated particles. Powder Technol. 407, 117683. https://doi.org/10.1016/j.powtec.2022.117683

Liu, Y., Zhang, Q., Liu, R., 2021. Effect of particle size distribution and shear rate on relative viscosity of concentrated suspensions. Rheol. Acta 60, 763–774. https://doi.org/10.1007/S00397-021-01301-4

Logos, C., Nguyen, Q.D., 1996. Effect of particle size on the flow properties of a South Australian coal-water slurry. Powder Technol. 88, 55–58. https://doi.org/10.1016/0032-5910(96)03103-8

Luo, L., Ingrid T., 2018. Experimental investigation of particle agglomeration effects on slurry settling in viscous fluid. Transp. Porous Med. 2, 333-352. https://doi.org/10.1007/s11242-017-0956-3

Mangesana, N., Chikuku, R.S., Mainza, A.N., Govender, I., Van Der Westhuizen, A.P., Narashima, M., 2008. The effect of particle sizes and solids concentration on the rheology of silica sand based suspensions. J. South. African Inst. Min. Metall. 108, 237–243.

Michaelides, E., Crowe, C.T., Schwarzkopf, J.D., 2016. Multiphase Flow Handbook. CRC Press, New York.

Mwale, A.H., Musonge, P., Fraser, D.M., 2005. The influence of particle size on energy consumption and water recovery in comminution and dewatering systems. Miner. Eng. 18, 915-926. https://doi.org/10.1016/j.mineng.2005.02.014

Ndlovu, B., Becker, M., Forbes, E., Deglon, D., Franzidis, J.P., 2011. The influence of phyllosilicate mineralogy on the rheology of mineral slurries. Miner. Eng. 24, 1314–1322. https://doi.org/10.1016/J.MINENG.2011.05.008

Ohki, A., Fukuda, S., Naka, K., Maeda, S., 1996. Studies on coal slurry fuel (part 4) effects of additive and particle size distribution on characteristics of coal-water mixture (CWM). Sekiyu Gakkaishi (Journal Japan Pet. Institute) 39, 129-36. https://doi.org/10.1627/jpi1958.39.129

Phillips, R.J., Armstrong, R.C., Brown, R.A., Graham, A.L., Abbott, J.R., 1992. A constitutive equation for concentrated suspensions that accounts for shear-induced particle migration. Physics of Fluids 1, 30-40. https://doi.org/10.1063/1.858498

Prasad, V., 2024. Influence of rheology on the hydraulic conveying of red mud slurries through the pipeline for eco-friendly and safe disposal. Part. Sci. Technol. 42, 1073-1084. https://doi.org/10.1080/02726351.2024.2320103

Prasad, V., Mehrotra, S.P., Thareja, P., 2019. Influence of additives, particle size, and incorporation of coarse particles on the shear rheology of concentrated Indian coal ash slurries.

Asia-Pacific J. Chem. Eng. 14, e2358. https://doi.org/10.1002/apj.2358

Rawat, A., Singh, S.N., Seshadri, V., 2019. Variation of physical and rheological properties of fly ash slurries with particle size and its effect on hydraulic transportation at high concentrations. Part. Sci. Technol. 37, 151-160. https://doi.org/10.1080/02726351.2017.1352636

Senapati, P.K., Mishra, B.K., 2012. Design considerations for hydraulic backfilling with coal combustion products (CCPs) at high solids concentrations. Powder Technol. 229, 119–125. https://doi.org/10.1016/j.powtec.2012.06.018

Senapati, P.K., Mishra, B.K., Parida, A., 2013. Analysis of friction mechanism and homogeneity of suspended load for high concentration fly ash & bottom ash mixture slurry using rheological and pipeline experimental data. Powder Technol. 250, 154–163. https://doi.org/10.1016/j.powtec.2013.10.014

Senapati, S., Pothal, J.K., Mohanty, A., 2019. Effect of particle size distribution on rheology of high concentration limestone–water slurry for economic pipeline transportation. Part. Sci. Technol. 37,707-715. https://doi.org/10.1080/02726351.2018.1436103

Singh, H., Kumar, S., Mohapatra, S.K., Prasad, S.B., Singh, J., 2021. Slurryability and flowability of coal water slurry: Effect of particle size distribution. J. Clean. Prod. 323, 129183. https://doi.org/10.1016/J.JCLEPRO.2021.129183

Singh, M.K., Ratha, D., Kumar, S., Kumar, D., 2016. Influence of Particle-Size Distribution and Temperature on Rheological Behavior of Coal Slurry. Int. J. Coal Prep. Util. 36, 44–54. https://doi.org/10.1080/19392699.2015.1049265

Sofrá, F., Boger, D. V., 2002. Environmental rheology for waste minimisation in the minerals industry. Chem. Eng. J. 86, 319–330. https://doi.org/10.1016/S1385-8947(01)00225-X

Standard I. IS 2386-3, 1963. Methods of test for aggregates for concrete, Part 3: Specific gravity, density, voids, absorption and bulking, New Delhi: Indian Standard.

Swamee, P.K., Aggarwal, N., 2011. Explicit equations for laminar flow of Bingham plastic fluids. J. Pet. Sci. Eng. 76, 178-184. https://doi.org/10.1016/j.petrol.2011.01.015

Zhao, L.A., Jian, C., Cai, R., He, P., 2024. Study of rheological parameters due to coal particle size change in pipeline transported coal slurry. Sci. Rep. 14, 29333. https://doi.org/10.1038/s41598-024-79696-2

Zhu, Z., Xiong, X., Liang, C., Zhao, M., 2018. On the flocculation and settling characteristics of low-and high-concentration sediment suspensions: effects of particle concentration and salinity conditions. Environ. Sci. Pollut. Res. 14, 14226-14243. https://doi.org/10.1007/s11356-018-1668-0

Received 8 October 2025
Accepted 17 December 2025